# Eagle syndrome: tissue characteristics and structure of the styloid process

Ruben D. de Ruiter[1] (iD), Sanne Treurniet[1], Nathalie Bravenboer[2], Björn Busse[3,4],
Jan Jaap Hendrickx[5], Jeroen C. Jansen[6], Leander Dubois[7], Willem H. Schreuder[7], Dimitra Micha[8],
Bernd P. Teunissen[9], Pieter G.H.M. Raijmakers[9], Elisabeth M.W. Eekhoff*,[1],
Felix N. von Brackel[3,4] (iD)

[1]Department of Internal medicine, Endocrinology and Metabolism, Rare bone disease center, Amsterdam University Medical Centers, Vrije Universiteit, Amsterdam Movement Sciences, 1081 HV Amsterdam, The Netherlands
[2]Bone and Calcium Metabolism Lab, Department of Clinical Chemistry, Amsterdam University Medical Centers, Vrije Universiteit, Amsterdam Movement Sciences, 1081 HV Amsterdam, The Netherlands
[3]Department of Osteology and Biomechanics, University Medical Center Hamburg-Eppendorf, 22529 Hamburg, Germany
[4]Interdisciplinary Center for Interface Research (ICCIR), University Medical Center Hamburg-Eppendorf, 22529 Hamburg, Germany
[5]Department of Otolaryngology, Head and Neck Surgery, Amsterdam University Medical Centers, Vrije Universiteit, 1081 HV Amsterdam, The Netherlands
[6]Department of Otolaryngology, Leiden University Medical Center, 2333 ZA Leiden, The Netherlands
[7]Department of Oral and Maxillofacial Surgery, Amsterdam University Medical Centers, 1081 HV Amsterdam, The Netherlands
[8]Department of Human Genetics, Amsterdam University Medical Centers, Vrije Universiteit, 1081 HV Amsterdam Reproduction and Development, Amsterdam, The Netherlands
[9]Department of Radiology and Nuclear Medicine, Amsterdam University Medical Centers, 1081 HV Amsterdam, The Netherlands

*Corresponding author: Elisabeth M.W. Eekhoff, Department of Internal medicine, Endocrinology and Metabolism, Rare bone disease center, Amsterdam University Medical Centers, Vrije Universiteit, Amsterdam Movement Sciences, De Boelelaan 1117, 1081 HV Amsterdam, The Netherlands (emw.eekhoff@amsterdamumc.nl)

## Abstract

Eagle syndrome is a bone disease where elongation of the styloid process leads to throat and neck pain, and in severe cases neurovascular symptoms such as syncope and neuralgia. The pathophysiology of Eagle syndrome is poorly understood with various theories having been proposed how this elongation is caused. To better understand the pathophysiology, we performed a work-up in 6 patients presenting with Eagle syndrome. Patients mainly presented with pain on turning the neck (100%), foreign body sensation (67%), tension in the neck (67%), and dysphagia (50%). The typical length of the styloid process ranges from 25 to 30 mm; however, [$^{18}$F]NaF (sodium fluoride) PET/CT showed elongated styloid processes with an average length of $52.1 \pm 15.6$ mm (mean $\pm$ SD) with increased turnover at the base of one of the styloid processes. The removed styloid processes were further examined by histology, micro-CT, quantitative backscatter electron imaging (qBEI), Fourier transform infrared spectroscopy (FTIR), and circularly polarized light imaging. Histology revealed one case of a fractured styloid process healing through callus formation and one case of pseudarthrosis. Bone mineral density and mineralization was similar in the styloid processes when compared to cortical bone samples derived from the mandibular bone of different patients. Circular polarized light microscopy showed a collagen orientation in the styloid process comparable to the cortical bone samples with a distinct separation of collagen structure between the mineralized structure and the surrounding soft tissue with FTIR analysis demonstrating a typical composition of bone. This altogether suggests that the elongated styloid processes in Eagle syndrome are mature bone, capable of endochondral repair, possibly growing from the base of the process through endochondral ossification, rather than being a form of secondary calcification of the stylohyoid ligament as previously postulated.

**Keywords:** bone histomorphometry, bone QCT/$\mu$CT, Eagle syndrome, matrix mineralization, [18F]NaF PET

## Introduction

In 1937, Watt Eagle reported 2 cases of styloid process elongation in patients who experienced symptoms post-tonsillectomy. Partial surgical removal of the elongated processes successfully relieved symptoms in both patients.[1] Before the publication of Eagle, elongation of the styloid process—only found on autopsy reports—was viewed as an anatomical curiosity. After Eagle described the elongation of the styloid process coinciding with symptoms such as pain in the neck, pharynx, or jaw region, restriction of neck rotation,

sensation of a foreign body in the pharynx, dysphagia and increased salivation, it became known as Eagle syndrome.[1,2]

The styloid process originates from the petrous part of the temporal bone and typically ranges between 25 and 30 mm long, but anatomical variation in the length is quite common.[1,3] Elongation of the styloid process is often asymptomatic and seen as an incidental finding on X-rays. The reported prevalence of Eagle syndrome varies between studies.[4,5] Eagle himself estimated the prevalence of an elongated styloid process in the general population to be 4%, with 4% of

those causing problems.[1,6] More recently, in a survey of 400 orthopantomograms, 291 patients were identified with a styloid process that was considered elongated of which 9.6% had symptoms constituting Eagle syndrome. Other estimates put the prevalence of Eagle syndrome between 4% and 10.3%,[7] making this altogether possibly a relatively common disorder, insufficiently recognized by clinicians.

Several mechanisms have been suggested to cause the elongation of the styloid process. The first proposes that the elongation of the styloid process is primarily caused by bone growth inside the styloid process. This growth can be triggered by a local trauma close to the process, such as the tonsillectomy suggested by Watt Eagle himself.[1] In a broader sense, growth of the styloid process can be induced by the mechanical force exerted by the stylohyoid ligament on the process over time, with a traumatic event perhaps exacerbating this growth. The second theory proposes that the elongation is caused by transformation of the stylohyoid ligament, either through secondary calcification of the ligament or by osseous transformation of persistent mesenchymal elements derived from the Reichert's cartilage in the stylohyoid ligament.[5,8]

Two types of Eagle syndrome have been described based on their presenting symptoms. In the classic type, elongation of the styloid process causes pain in the neck aggravated by chewing and yawning with a persistent foreign body sensation in the throat. In the carotid type, elongation of the styloid process exerts pressure on the neurovascular structures in the neck, causing neurological and vascular symptoms such as headaches, syncope, and other related symptoms. A recent microcomputed tomography study by Heim et al. attempted to define these 2 disease types further, linking the presenting symptoms and structural features of 10 Eagle syndrome patient biopsies.[9] Type I (the classic type) was described as an elongation of the styloid process itself, while type II (the carotid type) was linked to an ossification of the stylohyoid ligament.[9] Thus, one type arising from growth at the temporal bone of the styloid process (since it exhibits trabecular bone) and the other through metaplasia of the stylohyoid ligament (without trabecular bone at the thin distal tip of the process).

We performed an extensive clinical work-up in 6 patients with Eagle syndrome, using a [$^{18}$F]NaF (ie fluorine-18-labeled sodium fluoride) PET/CT scan and DXA scan to assess the presence of other features possibly related to increased bone turnover or high bone mass. After surgery, we performed in-depth tissue analysis with micro-computed tomography (micro-CT), quantitative backscatter electron imaging (qBEI), Fourier transform infrared spectroscopy (FTIR), and circularly polarized light microscopy (CPL) analysis to better characterize the tissue properties of the removed styloid process.

## Materials and methods
### Patients

After confirmation of Eagle syndrome by CT, patients were asked to participate in a more extensive work-up and consented to in-depth analysis of the removed styloid processes after surgery. Before the study, approval for the research was provided by the Medical Ethical Committee of the Amsterdam University Medical Centers, location VUmc (Registration Number 2017.346). All patients were fully informed and signed an informed consent form for the use of their tissue and data in the present study. Control samples were sourced from a separate study in which mandibular bone biopsies were obtained from patients undergoing a dental implant procedure

with a trephine (Registration Number 2005.128). All methods were performed in accordance with the relevant guidelines and regulations.

### [$^{18}$F]NaF PET/CT

A [$^{18}$F]NaF PET/CT was performed prior to the surgical procedure. Sixty minutes after the injection of $98.3 \pm 22.4$ (mean $\pm$ SD) MBq of [$^{18}$F]NaF, patients were scanned on the Ingenuity PET/CT scanner (Philips Healthcare). Initially, a low-dose CT scan was performed for the purpose of attenuation and localization. This was followed by a whole body scan (2 min per bed position, 8 bed positions). The Philips Ingenuity system uses an iterative reconstruction algorithm with rotationally symmetric volume elements ordered subsets time-of-flight (blob-os-tf) for the whole body scans.[10] The maximum standardized uptake value (SUV$_{max}$) and maximum Hounsfield units (HU$_{max}$) were measured at the base and tip of the styloid process on both sides on the PET/CT images.

### DXA scan

DXA scan (Hologic Discovery A, Hologic Inc.) was used to measure the areal bone mineral density in g/cm$^2$ of the TH and FN of the non-dominant hip and the LS, measuring the first 4 lumbar vertebrae (L1-L4). Calibration scans were acquired daily following the International Society for Clinical Densitometry guidelines.[11]

### Histology

Samples were immediately transferred to a 4% formaldehyde solution following the surgical procedure. Following the protocol as previously outlined,[12] the samples were subsequently prepared and embedded in an oblique orientation creating a longitudinal histological section. All biopsies were then embedded in methyl-methacrylate (MMA) and prepared for histological examination. In brief, the bone samples underwent dehydration using an ascending alcohol series and were subsequently infiltrated with methyl methacrylate under controlled conditions. After embedding, the samples were sectioned to a thickness of 4 $\mu$m using a microtome, and subsequently subjected to von Kossa, toluidine blue, Masson-Goldner, Safranin-O, and Picrosirius red staining.

### Microcomputed tomography analysis

During the elective surgical procedure, the removed tissue was obtained for analysis. Samples were fixed in 70% ethanol. Micro-CT analysis was performed to assess the bone composition. Samples were scanned with a micro-CT system (Micro-CT 40, SCANCO Medical AG) at a spatial resolution of 15 $\mu$m. The system was calibrated weekly with a standardized phantom provided by the manufacturer. Gray values represent the local bone tissue mineral density, calibrated to the phantom. Volumes-of-interest were chosen by visual inspection. The threshold for tissue evaluation was set to 260 mgHA/cm$^3$. Due to its high variability in shape and size, only bone tissue mineral density (BMD; mgHA/cm$^3$) was measured. For analysis, the manufacturer's software was used. To provide a basis for comparison, we utilized cortical bone samples ($n = 6$) obtained from mandibular biopsies of individuals without bone disease but in needing dental implants.

### Quantitative backscattered electron imaging

Quantitative backscattered electron imaging was used to measure the bone mineral density distribution (BMDD) of

the styloid processes, as described elsewhere.[13] Measured BMDD of the styloid processes was compared to cortical control samples derived from the mandibular bone of separate patients. Briefly, polymethylmethacrylate (PMMA)-embedded specimens were cut and ground plane-parallel, and then coated with a defined carbon layer for further imaging. The samples were mounted in a scanning electron microscope (Crossbeam 340, Zeiss AG). Imaging was carried out in backscatter mode at 20 keV and a constant working distance of 20 mm. A magnification level of 200× was chosen for acquiring the quantitative images. The resulting images were recorded as 8-bit images, with brightness and contrast calibrated against aluminum and carbon standards set at 4.8 and 222, respectively. Image analysis was performed using a custom-built MATLAB script,[13] with data derived from the analysis of the grayscale value distribution. Parameters such as total mineral density (TMD), mean calcium concentration ($Ca_{mean}$), most frequent calcium concentration based on calcium peak intensity ($Ca_{peak}$), and mineralization heterogeneity (quantified by standard deviation and full width at half maximum) were determined.

### Circularly polarized light microscopy

CPL microscopy was employed to visualize the predominant collagen fiber orientation in bone, as previously described.[14] Collagen fibers aligned parallel to the light beam appear dark, while those oriented perpendicular to the light beam appear bright. Thus, bright areas indicate longitudinal collagen orientation in the direction of the bone, while dark regions suggest collagen orientation transverse to the primary axis of the dissected samples. An Olympus BX-61 microscope equipped with circular polarizing filters was used for the imaging process. Histological sections of 4 $\mu$m thickness, stained using toluidine blue prior to analysis, were used. For signal enhancement, additional sections were stained with picrosirius red staining (images appear yellowish, greenish) in comparison to Toluidine blue-stained sections (appear blueish).

### Fourier transform infrared spectroscopy

FTIR spectra were measured at a Spotlight 400 (PerkinElmer) in attenuated total reflection-mode (ATR) over a spectral range of 4000 to 570 $cm^{-1}$ wave numbers at a resolution of 4 $cm^{-1}$ and with 16 scans per probing. An automated atmospheric correction (PerkinElmer) and background subtraction were applied to the measured samples, ensuring no influence from atmospheric factors such as water vapor, etc. Five of 6 samples were probed, since one sample did not exhibit sufficient material left after histologic processing.

### Statistical analysis

Results are presented as mean ± SD. TMD, $Ca_{Mean}$, $Ca_{Peak}$, $Ca_{Low}$, $Ca_{High}$, StdDev were also compared between the styloid process samples and cortical control samples through a standard Student's t-test. Similarly, $SUV_{max}$ at the base and tip of the affected styloid process was compared to the uptake on the contralateral side through a standard student's t-test. Linear regression was used to study the possible correlation between $SUV_{max}$ at the base of the process and the length of the process.
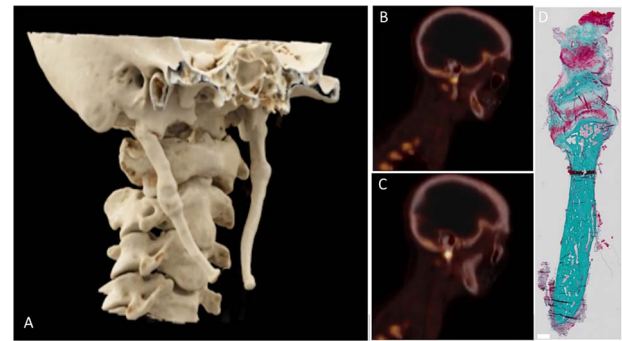


**Figure 1.** 3D reconstruction from CT image, sagittal [18F]NaF PET/CT images, and microscopic detail image of patient 2. The styloid process was elongated bilaterally (A) with the right styloid process causing symptoms. Increased [18F]NaF uptake was observed at the base of the styloid process (B, C) with a pseudoarthrosis being visible in the histological detail of the styloid process (D).

## Results

### Patient characteristics

Six patients were referred to the hospital with suspicion of Eagle syndrome. Symptoms of the respective patients are listed in Table 1. All patients reported pain when turning the neck. Other common symptoms were a foreign body sensation in the throat, dysphagia, and increased saliva production. One patient reported a tonsillectomy in their patient history, which was performed when the patient was still a child. All patients reported a decrease or even complete relief of their symptoms after surgery.

### Radiology

Patients underwent DXA scan and [18F]NaF PET/CT prior to surgery. Table 2 lists the DXA scan results, the length of the styloid process measured from the base attached to the petrous part of the temporal bone to the tip on the sagittal CT images, and the uptake and density of the process at the base and tip as measured on the PET/CT. DXA scan (mean ± SD) Z-scores were −0.96 ± 1.4 at the LS, Z-score of the TH was 0.12 ± 0.50, while the FN was at 0.08 ± 0.79.

The mean $SUV_{max}$ at the base of the styloid process on the affected side was 3.88 (± 4.6) with a mean $SUV_{max}$ of 1.74 (±0.50) on the contralateral side ($p$=0.33). The mean $SUV_{max}$ at the tip of the styloid process on the affected side was 1.31 (± 0.84) with a mean $SUV_{max}$ of 1.04 (± 0.48) on the contralateral side ($p$=0.53). Figure 1 shows a 3D rendition of the styloid process in one patient, combined with an example of a PET/CT scan, demonstrating increased uptake at the base of the styloid process together with the histological sample. The $SUV_{max}$ measured at the base of the styloid process showed only a low correlation with the length of the styloid process ($r$ = 0.46).

### Structural and compositional tissue analysis
#### Overview histology

The removed styloid processes were composed of compact bone with a marrow space (Figure 2). Among these samples, 3 exhibited indications of previous fractures, as evidenced by the presence of pseudarthrosis and callus formation (Figure 3). In the marrow cavity of the styloid, trabecular structures were evident (Figures 2 and 3, Figure S1). No regions of abnormal bone growth were visible (Figure 2). In the case of callus formation, an increased styloid width was

**Table 1.** Patient characteristics and presenting symptoms constituting Eagle syndrome.

|  | 1 | 2 | 3 | 4 | 5 | 6 | Total |
|---|---|---|---|---|---|---|---|
| Gender | ♀ | ♂ | ♀ | ♀ | ♂ | ♂ |  |
| Age | 44 Y | 57 Y | 42 Y | 54 Y | 37 Y | 36Y |  |
| Side of elongation | Right | Right | Bilateral | Left | Left | Left |  |
| Tonsillectomy |  |  |  |  |  | Y | (1/6) 16% |
| Tooth extraction | Y |  |  |  | Y |  | (2/6) 33% |
| Tension in the neck | Y |  | Y | Y | Y |  | (4/6) 67% |
| Pain on turning head | Y | Y | Y | Y | Y | Y | (6/6) 100% |
| Limited jaw opening | Y |  |  |  |  | Y | (2/6) 33% |
| Swelling neck |  | Y | Y | Y |  |  | (3/6) 50% |
| Foreign body sensation | Y | Y |  | Y |  | Y | (4/6) 67% |
| Dysphagia/odynophagia | Y | Y | Y |  |  |  | (3/6) 50% |
| Dysphonia | Y | Y |  | Y |  |  | (3/6) 50% |
| Sialorrhea |  | Y |  | Y |  | Y | (3/6) 50% |
| Neurological symptoms | Y | Y |  |  |  |  | (2/6) 33% |
| Auditory symptoms | Y |  | Y |  |  |  | (2/6) 33% |

Y, yes (symptom present); ♀, female; ♂, male.

**Table 2.** Length and uptake of the styloid processes as measured on the [$^{18}$F]NaF PET/CT reconstructed images.

| Patient | 1 | 2 | 3 | 4 | 5 | 6 |
|---|---|---|---|---|---|---|
| Symptomatic side | Right | Right | Bilateral | Left | Left | Left |
| LS | −0.5/−0.1 | −1.6/−1.1 | NA | 1.2/1.4 | −1.2/−1.2 | −2.7/−2.7 |
| T-score/Z-score |  |  |  |  |  |  |
| TH | 0.5/−0.2 | −0.6/−0.2 | NA | 0.5/1 | −0.1/0 | −0.1/0 |
| T-score/Z-score |  |  |  |  |  |  |
| FN | −1.2/−0.8 | −1.5/−0.6 | NA | 0.1/1 | −0.3/0.1 | 0.3/0.7 |
| T-score/Z-score |  |  |  |  |  |  |
| Right side |  |  |  |  |  |  |
| Length (mm) | 28.1 | 44.8 | 73.6 | 45.6 | 43.1 | 66.3 |
| HU$_{max}$ (base-tip) | 795-325 | 1433-486 | 1523-648 | 913-670 | 941-614 | 1454-854 |
| SUV$_{max}$ (base-tip) | 2.30-1.83 | 2.17-0.84 | 14.23-2.78 | 1.61-0.72 | 1.13-0.67 | 1.45-0.77 |
| Left side |  |  |  |  |  |  |
| Length (mm) | 14.1 | 30.6 | 70.3 | 47.2 | 49.6 | 51.7 |
| HU$_{max}$ (base-tip) | 807-358 | 1455-535 | 1641-987 | 879-409 | 1431-685 | 1499-923 |
| SUV$_{max}$ (base-tip) | 2.27-1.80 | 2.24-1.23 | 2.77-1.79 | 1.43-0.81 | 1.36-0.59 | 2.87-0.56 |

NA, not available; HU, Hounsfield unit; SUV, standardized uptake value.

observed with bone marrow and trabecularization evident (Figure 2C–D, I–J, and O–P, Figure 3). One case exhibited a pseudarthrosis (Figures 2D, J, and P, and 3C and D). In the case of pseudarthrosis, cartilage tissue was visible and showed the typical restructuring in the CPL (Figures 2P and 3D). Additionally, one sample (Figure 2A, G, and M) did exhibit signs of cartilaginous remnants in the bone volume of the sample. These remnants correlate with the highly mineralized tissue volumes seen in $\mu$CT imaging (Figure 4C–E). This was only evident for one sample. Safranin-O staining did indicate a fibrous tissue surrounding the tip of one sample (Figure 2L) that was slightly saturated with proteoglycans, as evidenced by a faint reddish staining.

### Circular polarized light microscopy analysis

CPL imaging revealed no significant deviations in the collagen alignment in the samples imaged (Figure 2M–R, Figure S2). Collagen arrangement was respecting the osteonal plywood structure. Bright areas of the CPL images indicate the collagen to be oriented in the osteonal direction of the longitudinal axis of the styloid in picrosirius red staining. Importantly, at the tip, an interface was visible (see Figure S2), indicating a distinct separation of collagen structure between the mineralized structure and the surrounding soft tissue. This suggests that the styloid process exhibits bone collagen alignment rather than a partially mineralized ligamentous structure. Moreover, there is no gradual transition of structures from the process to the surrounding soft tissues; instead, a surrounding fibrous tissue appears unstructured. Collagenous restructuring was observed in the case of pseudarthrosis (Figure 3C and D).

### Micro-computed tomography-analysis

Detailed tissue analysis using micro-computed ($\mu$CT)-imaging indicated a distinct similarity between the styloid process and control skull bone samples with no differences in TMD (Figure 4A) for the whole available bone volume comparison. Notably, micro-CT imaging revealed volumes of highly mineralized tissue in the styloid processes (Figure 4C–E) for the aforementioned sample, with inclusion of Safranin-O red positive areas. Correlative imaging indicates high mineral content within the region of Safranin-O positive red staining. Due to the high variability in shape and size of the styloid processes, no evaluation of structural parameters was valid.

### qBEI analysis

The mineralized structure of the styloid processes appeared cortical bone-like with an evenly distributed matrix mineralization (Figure 5A and B). A clear edge of mineralized bone tissue was visible at the distal tip of the styloid process (Figure 5A). In the area of pseudarthrosis, there
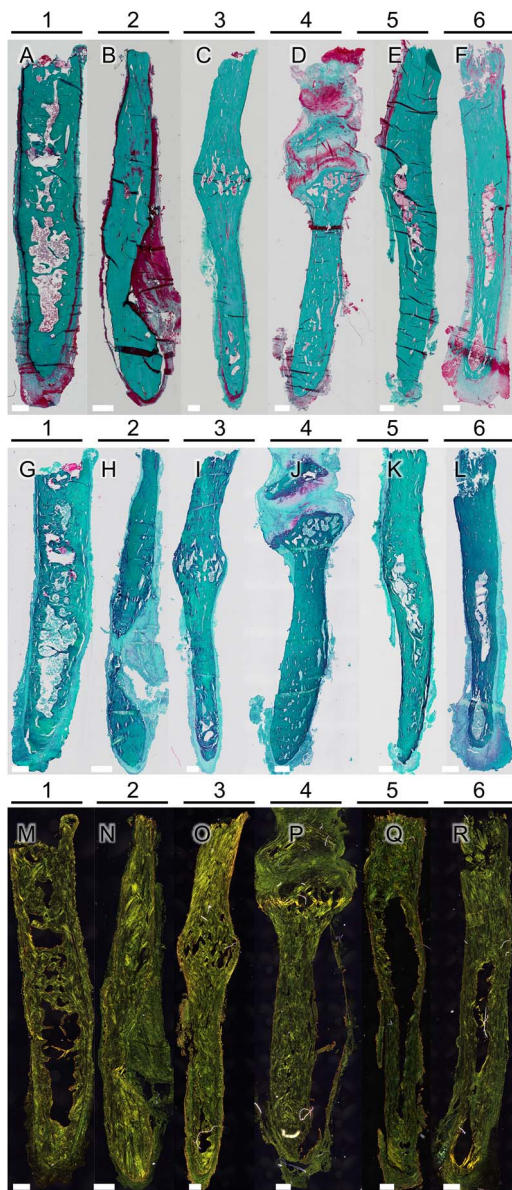
**Figure 2.** Microscopic images of full biopsies generated for each sample after Masson-Goldner staining (A–F). Bars for scale are 500 $\mu$m. No epiphysis is visible, which indicates no abnormal site of bone growth. In addition, Safranin-O staining revealed remnants of cartilaginous tissue in one sample (G), while the other samples (H-L) showed no evidence of cartilage within the bone tissue, except for one sample (J) exhibiting cartilage formed at a pseudarthrosis, possibly following a fracture of the styloid process. One sample exhibited reddish staining (L) in the surrounding soft tissue, which may be a sign of proteoglycans or inflammation. Picrosirius red staining (M–R) was utilized to enhance the circularly polarized light (CPL) signal for imaging collagen alignment. In all samples, a plywood-like structure, including osteonal structures, was observed.

was subchondral hypermineralization visible in the qBEI (Figure 5C). Structures of osteonal bone in a plywood arrangement were evident in qBEI imaging (Figure 5D and E). Additionally, signs of bone remodeling were evident in qBEI (Figure 5D) as evidenced by secondary osteons (Figure 5D). Furthermore, areas of woven bone structure were evident in qBEI imaging, and osteocyte lacunae were uniformly present throughout the samples, as illustrated in Figure 5E and F. This distribution is consistent with normal bone morphology,

indicative of bone tissue. Consistent with the TMD in micro-CT analysis, qBEI showed no differences in mean mineralization parameters compared to control skull bone samples (Figure 5G–L), although there was a large variation among the Eagle syndrome tissue samples compared to the control group.

### FTIR spectroscopy analysis

FTIR analysis (Figure 6) confirmed the typical tissue composition of bone, marked by the presence of collagen (as indicated by the amide I and amide II peaks) and hydroxyapatite (as highlighted by the phosphate and carbonate peaks). Spectra were measured across a radius of 1.25 mm. The minor peak at 1700 cm$^{-1}$ corresponds to the PMMA embedding medium.

## Discussion

Eagle syndrome remains a condition with an unclear underlying pathophysiology. We performed a comprehensive clinical investigation of 6 patients with Eagle syndrome followed by structural and compositional tissue analyses of the styloid processes after surgical removal demonstrating the styloid process to be mature bone with functional bone metabolism. The mineralization patterns observed in the styloid process are similar to those found in cortical control samples. Furthermore, the collagen orientation within the bone of the styloid processes aligns longitudinally with the orientation of the styloid process and exhibits osteonal structures. These findings suggest that the growth occurring in the styloid process follows a coordinated process rather than resulting from secondary mineralization of ligamentous tissues.

Different theories about the pathophysiological process of styloid elongation and categorization have been discussed in literature[1,8,15] including trauma to be a triggering factor.[16] In our series, 3 of the 6 patients reported no history of neck trauma or surgery, with 2 patients reporting (multiple) dental extractions and one patient reporting adenoidectomy as a child. Because an overlong process could be interpreted as excessive bone growth, the possibility was considered that individuals with Eagle syndrome might exhibit other characteristics of high bone mass conditions, such as osteopetrosis or conditions associated with other benign bony outgrowths such as multiple osteochondromas. One patient showed intense [$^{18}$F]NaF uptake and extraskeletal ossification around the vertebrae, but this was more likely due to degenerative arthrosis. Additionally, the bone density was found to range from osteopenic to normal and none of the patients presented high bone mass. Genetic analysis was also considered to identify variants possibly contributing to the development of Eagle syndrome. Coincidentally, a whole exome sequencing was performed in one patient without yielding any relevant variants. In short, no manifesting signs of a systemic change in bone metabolism were found, suggesting that the elongation of the styloid causing Eagle syndrome may result from local factors during the individual's lifetime rather than systemic bone affective metabolic reasons.

Several classifications of the Eagle syndrome have been proposed, either through presenting symptomology or by suspected underlying pathophysiology.[9] Upon examination of the presenting symptoms of our cohort, most patients reported symptoms linked to the classic type (pain in the neck when chewing or yawning and a foreign body sensation) but some
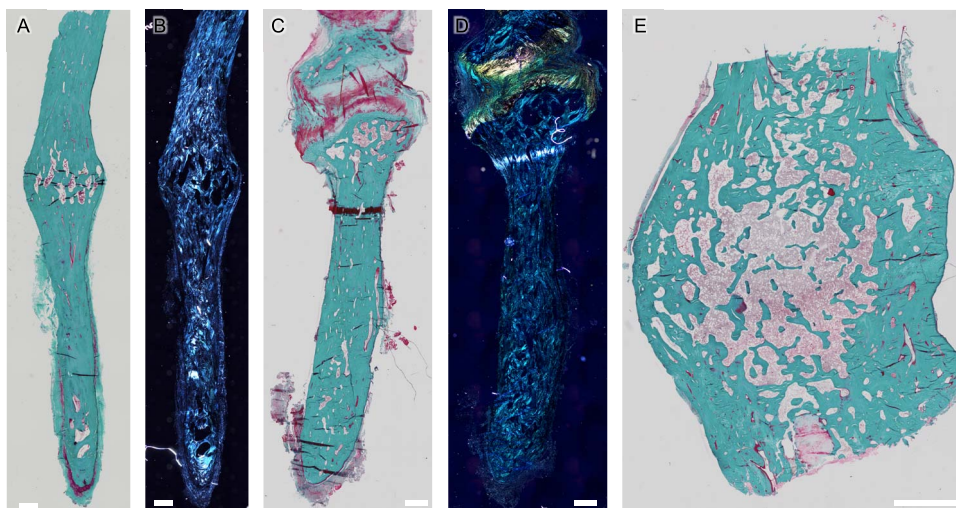
**Figure 3.** Details of the full biopsies after Masson-Goldner staining (A, C, E) and CPL microscopic imaging (B, D). Bars for scale are 500 $\mu$m. Signs of past fractures with callus formation (patient 3; A and B, E) and formation of a pseudarthrosis are visible (patient 4; C and D). Within the region of callus formation, trabecular bone is evident (A, C, E).
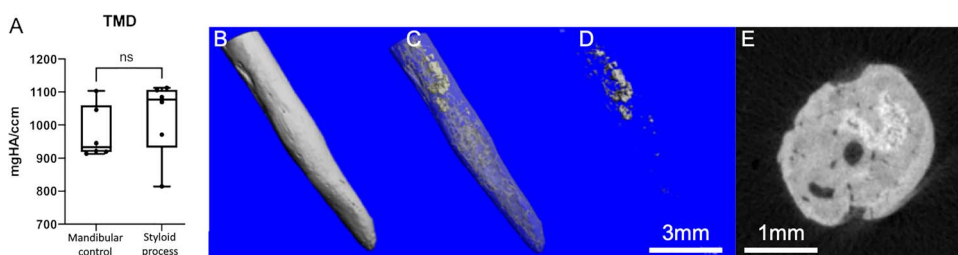


**Figure 4.** Micro-CT analysis. No difference was detected between the groups with respect to TMD (A). A full 3D representation of a sample (patient 2) is shown in (B). In this sample, highly mineralized volumes were found (matching the sample with remnants of cartilage in safranin-O staining), as depicted in a fused image (C) depicting highly mineralized cores in light gray and inner marrow cavities. (D) Depicts the volume of highly mineralized tissue, also presented in cross-sectional view (E).

simultaneously reported neurovascular symptoms (syncope, auditory symptoms, dysphonia, dysphagia). As for classification, all biopsies exhibited structures of a central bone marrow space and trabeculae (Figure 2), yet to a significantly different extent (Figure 2A, D, and F vs Figure 2B, C, and E).

Our tissue analysis demonstrates that the tissue formed in Eagle syndrome comprises mature bone with its characteristic structures and osteocytes, rather than a form of secondary mineralized ligament (Figure 2). Histological analysis additionally revealed cortical structures, including osteonal assemblage. Furthermore, the presence of osteocyte lacunae throughout the bone further confirms the presence of mature bone tissue. Safranin-O staining revealed one sample incorporating cartilaginous tissue (Figure 2G), corresponding to the volumes of highly mineralized tissue presented in Figure 4C–E. However, this tissue is integrated into the bone volume and is not located at the tip. Therefore, it is indicative of non-remodeled bone. Additionally, the presence of proteoglycan content at the soft tissue around the tip of one sample may suggest inflammation, which has been discussed as partially responsible for heterotopic ossifications.[17] Fibrous tissue at the tip of the samples may reflect the growth into soft tissue. Furthermore, histological analysis revealed evidence of past fractures with signs of fracture healing as evidenced by callus formation with a widened bone diameter and marrow space (Figure 3), indicating a functional bone metabolism (Figure 3), as well as one case exhibiting

pseudarthrosis following a fracture, characterized by the development of a joint and the formation of subchondral, highly mineralized bone (Figure 5C). Therefore, our results suggest that the previously described types[9] are not mutually exclusive, with anatomical localization of the styloid process primarily causing any differences in presenting symptoms.

Micro-CT analysis further revealed that the bone tissue of the styloid process is comparable to cortical control bone samples regarding tissue mineral density (Figure 4). Remnants of highly mineralized bone tissue were also observed in the micro-CT analysis in one specific case (Figure 4C–E). These remnants are possibly leftover pieces of primary bone,[18] not resorbed during growth or remodeling.

Analysis of the BMDD with respect to heterogeneity and mean calcium concentration is in accordance with the micro-CT results (Figure 4). The mean calcium content between control samples and Eagle biopsies was not significantly different, indicating the composition of the processes being similar to skeletal bone tissue (Figure 5). An interface boundary can be distinguished in all samples between mineralized bone tissue and the surrounding tissue, indicating no subsequent or partial mineralization of ligamentous structures (Figures 2 and 5A). The samples show osteonal structures with lamellar configuration,[19] osteocyte lacuna, and even bone mineralization. Hypermineralization with respect to neighboring non-bony collagen/ cartilage was only visible in a case with pseudarthrosis (Figure 5C) in the subchondral bone, in line with
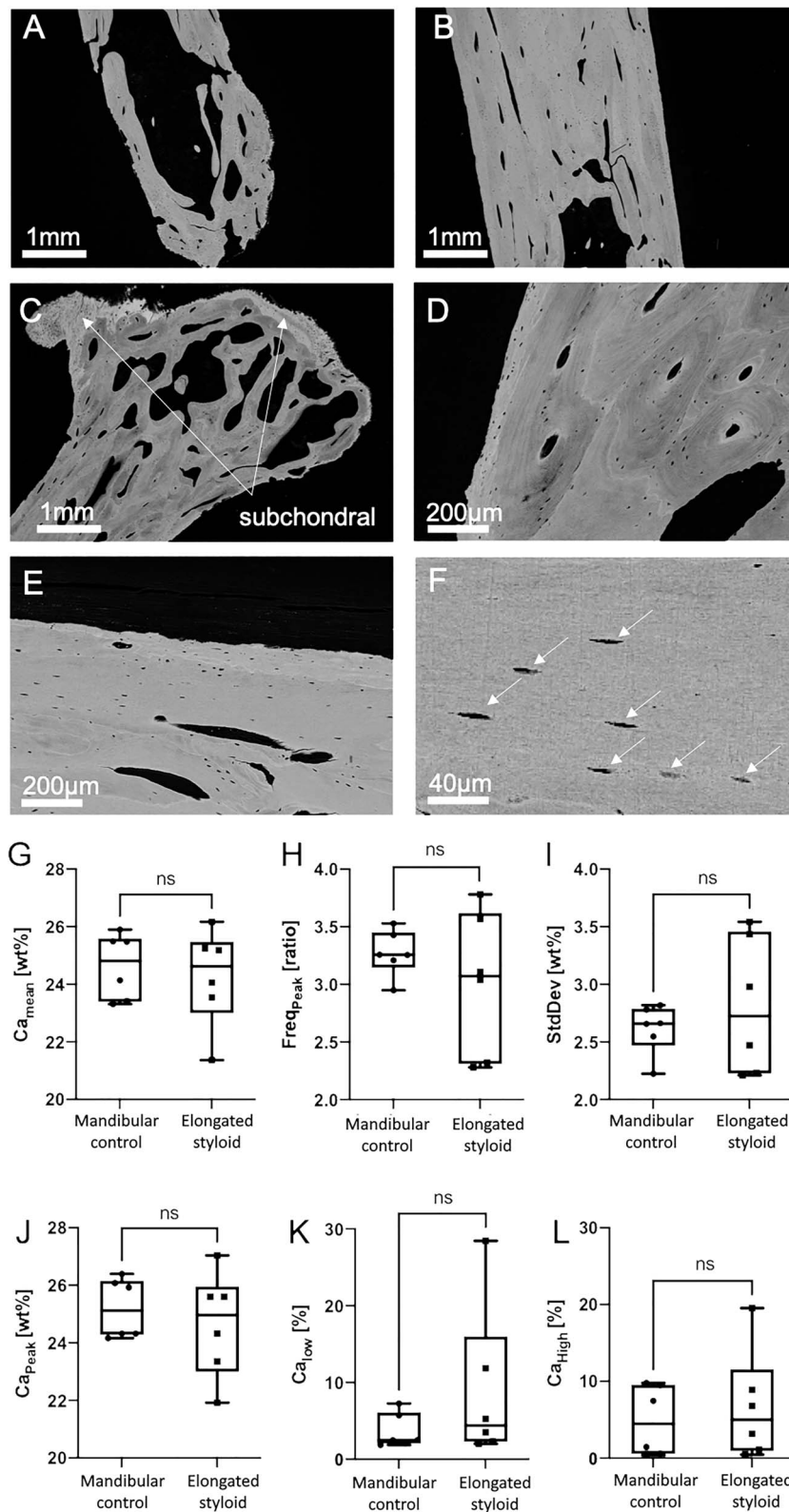
**Figure 5.** Quantitative backscattered electron imaging: The bone structure generally appears normal and comparable to cortical bone (patient 1; A and B). Within the inner volume of the tip, the trabecular structures are visible (A) as well as a defined edge marks the end of the mineralized tissue, indicating a clear boarder between bone and soft tissue. No mineralization gradient can be seen between center and outer volumes (A and B). Some areas of one sample exhibit highly mineralized bone, specifically in the subchondral region of the pseudarthrosis (patient 4; C), as known from the subchondral bone plate in other joints (also depicted in Figures 2D, J, and P and 3C and D). The tissue volume resembles typical structures of cortical bone, as seen in D and E. Osteocytes are present all over the bone tissue (patient 1; F), white arrows point to osteocyte lacuna. No differences with respect to mineral content were found in the Eagle samples compared to mandibular cortical control samples, measured by qBEI (Ca$_{Mean}$, Ca$_{Peak}$, Ca$_{Low}$, Ca$_{High}$, StdDev). However, a far more heterogeneous distribution of the mean values per specimen is present in case of the eagle specimens (G-L). No density gradient was seen ranging from the outer surface toward the center of the styloid process, as seen in C and the lower left of D. ns = not significant, Ca$_{mean}$ = calcium mean content, Freq$_{Peak}$ = frequency, StdDev = standard deviation, Ca$_{peak}$ = calcium peak, Ca$_{low}$ = calcium low, Ca$_{high}$ = calcium high.
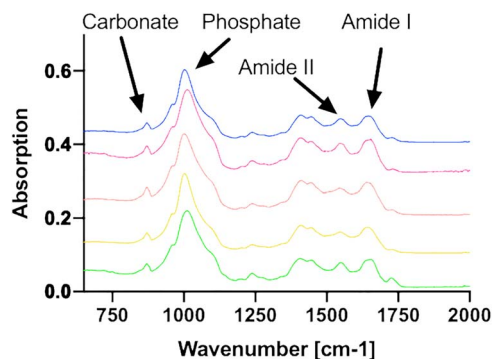
**Figure 6.** FTIR-spectroscopic composition analysis: all measured samples display a characteristic bone spectrum with prominent carbonate and phosphate peaks, indicating the presence of hydroxyapatite, which primarily comprises calcium and phosphate. Additionally, the presence of amide I and amide II peaks suggest the presence of the collagenous matrix. Therefore, it can be concluded that the primary constituent of the samples is bone tissue.

previous reports.[20] In addition, enclosed areas of woven bone show the originality of the bone and its formation. Spectroscopic analysis confirms the compositional similarities of the mineralized tissue in the styloid being comparable to typical bone tissue in other skeletal sites.[14,21] Taken together, this indicates the styloid process to be mature bone capable of a functional bone metabolism (including fracture healing) and not being primarily a consequence of secondary mineralization of a ligament.

During the embryonic period, most of the flat bones of the cranium are developed through intramembranous ossification; the temporal bone can be viewed as an exception. The tympanic ring and squamous portion of the temporal bone are formed through intramembranous ossification, whereas the petrous and styloid portions are formed through endochondral ossification.[22] As already mentioned, the presence of callus formation after a fracture in some samples demonstrates that the bone repair in the styloid process occurs through endochondral ossification. Given remnants of hypermineralized bone, this may indicate endochondral ossification where bone develops through a hyaline cartilage intermediate, which is infiltrated by chondroclasts and osteoblasts which start creating the bone shape by resorbing and replacing of the mineralized hyaline cartilage.[23] The specific region from which the styloid process originates remains unclear. In a histological analysis, Kim et al. showed increased expression of 70 kilodalton heat shock protein (HSP-70) and Heme-oxygenase 1 (HO-1), both cellular markers of mechanical stress, in the tip of the styloid process.[24] The tip of the styloid process simultaneously showed an increased expression of the bone turnover markers BMP-2, RANKL, osteonectin, and osteocalcin.[24] Based on the cellular morphology and Safranin-O staining in the present samples, no chondrocytes were identified at the tip of the styloid except one very small area in one sample (Figure 2G). The increased expression of these markers may be caused by the mechanical stimulation of the elongated bone and/or the attachment of the ligament transferring loads during motion, thus provoking a biochemical reaction of the bone and driving the primary elongation process. On the other hand, one [18F]NaF PET/CT showed substantially more uptake at the base of the styloid process than at the tip, inferring that the growth might instead originate at the base pushing the styloid further out. In this sense, growth of the styloid process

may be similar to growth in unilateral condylar hyperplasia, where growth at the base of the condyle causes a protrusion leading to mandibular asymmetry.[25,26] An alternative mechanism could be mechanical overstimulation at the base through the long lever of an extended processes, which stimulates the mechanoreactive bone and its metabolism. The styloid process exhibiting increased uptake at the base also revealed pseudarthrosis inferring this mechanical stimulation on the styloid process in vivo (Figure 1). A comprehensive analysis of the surrounding soft tissue at the tip was not feasible, as it was not removed during the surgical procedure and remained with the patient. Regrowth of the styloid process has not been reported after surgery, although a long-term radiological follow-up is lacking in Eagle syndrome.

Although this research provides valuable insights into the pathophysiology of Eagle syndrome, certain limitations should be acknowledged. First, the sample size was relatively small. We analyzed 6 patients, finding that all elongated styloid processes to be mature bone. It is possible that the previously proposed "secondary" mineralizing form is less common than the ossifying form, and therefore was simply missed in this sample size. Second, we only observed the patients presenting with Eagle syndrome for a short period and assessment of the bone metabolism through [18F]NaF PET/CT was only performed once. Should bone metabolism in the styloid process vary over time, this could be missed by the [18F]NaF PET/CT. A longer period of follow-up, ideally combined with radiological imaging, could establish the growth of the styloid process over time, whether or not the styloid process is capable of regrowth after surgery and from which region the styloid process grows.

In conclusion, our structural and compositional analysis of the elongated styloid process in 6 Eagle syndrome patients shows that the tissue in styloid processes is composed of mature bone. The elongated bony outgrowth represents mature bone, which is capable of endochondral ossification upon fracturing. The lack of a predisposition toward increased bone turnover in these patients and a normal bone density in DXA measurements points to a localized mechanism underlying the pathological styloid elongation rather than a systemic process.

## Acknowledgments

## Author contributions

Ruben D. de Ruiter (Data curation, Formal analysis, Investigation, Project administration, Validation, Writing—original draft, Writing—review & editing), Sanne Treurniet (Conceptualization, Data curation, Writing—original draft, Writing—review & editing), Nathalie Bravenboer (Conceptualization, Investigation, Writing—review & editing), Björn Busse (Conceptualization, Supervision, Writing—review & editing), Jan Jaap Hendrickx (Data curation, Writing—review & editing), Jeroen C. Jansen (Data curation, Writing—review & editing), Leander Dubois (Data curation, Writing—review & editing), Willem H. Schreuder (Data curation, Writing—review & editing), Dimitra Micha (Investigation, Writing—review & editing), Bernd P. Teunissen (Investigation, Visualization, Writing—review & editing), Pieter G.H.M. Raijmakers (Investigation, Supervision, Writing—review & editing), Elisabeth M.W. Eekhoff (Conceptualization, Data curation, Supervision, Writing—review & editing), and Felix N. von Brackel (Conceptualization, Data curation, Formal analysis, Investigation, Methodology, Supervision, Writing—review & editing).

## Supplementary material

Supplementary material is available at *JBMR Plus* online.

## Funding

## Conflicts of interest

No authors have conflicts of interest to disclose.

## Data availability

The data underlying this article will be shared on reasonable request to the corresponding author.

## References

1. Eagle WW. Elongated styloid process; further observations and a new syndrome. *Arch Otolaryngol (1925)*. 1948;47(5):630–640. https://doi.org/10.1001/archotol.1948.00690030654006

2. Eagle WW. Symptomatic elongated styloid process; report of two cases of styloid process-carotid artery syndrome with operation. *Arch Otolaryngol (1925)*. 1949;49(5):490–503. https://doi.org/10.1001/archotol.1949.03760110046003

3. Jung T, Tschernitschek H, Hippen H, Schneider B, Borchers L. Elongated styloid process: when is it really elongated? *Dentomaxillofac Radiol*. 2004;33(2):119–124. https://doi.org/10.1259/dmfr/13491574

4. Nogueira-Reis F, de Oliveira RL, Fontenele RC, Freitas DQ, Tabchoury CPM. Prevalence and features of elongated styloid process on imaging studies: a systematic review and meta-analysis. *Clin Oral Investig*. 2022;26(2):1199–1215. https://doi.org/10.1007/s00784-021-04285-w

5. Murtagh RD, Caracciolo JT, Fernandez G. CT findings associated with Eagle syndrome. *AJNR Am J Neuroradiol*. 2001;22(7):1401–1402.

6. Eagle WW. Elongated styloid process; symptoms and treatment. *AMA Arch Otolaryngol*. 1958;67(2):172–176. https://doi.org/10.1001/archotol.1958.00730010178007

7. Assiri Ahmed H, Estrugo-Devesa A, Roselló Llabrés X, Egido-Moreno S, López-López J. The prevalence of elongated styloid process in the population of Barcelona: a cross-sectional study & review of literature. *BMC Oral Health*. 2023;23(1):674. https://doi.org/10.1186/s12903-023-03405-0

8. Rechtweg JS, Wax MK. Eagle's syndrome: a review. *Am J Otolaryngol*. 1998;19(5):316–321. https://doi.org/10.1016/S0196-0709(98)90005-9

9. Heim N, Warwas FB, Singer L, Kramer FJ, Bourauel C, Götz W. Differences in the osseous ultrastructure in 2 differing Etiologies of Eagle syndrome. A micro-CT study. *J Craniofac Surg*. 2023;34(5):e453–e458. https://doi.org/10.1097/SCS.0000000000009296

10. Popescu LM, Matej S, Lewitt RM. Iterative image reconstruction using geometrically ordered subsets with list-mode data; *2004 IEEE Nuclear Science Symposium and Medical Imaging Conference*. 2004. pp. 3536–3540.

11. Lewiecki EM, Binkley N, Morgan SL, et al. Best practices for dual-energy X-ray absorptiometry measurement and reporting: International Society for Clinical Densitometry Guidance. *J Clin Densitom*. 2016;19(2):127–140. https://doi.org/10.1016/j.jocd.2016.03.003

12. Hahn M, Vogel M, Delling G. Undecalcified preparation of bone tissue: report of technical experience and development of new methods. *Virchows Arch A Pathol Anat Histopathol*. 1991;418(1):1–7. https://doi.org/10.1007/BF01600238

13. Roschger P, Fratzl P, Eschberger J, Klaushofer K. Validation of quantitative backscattered electron imaging for the measurement of mineral density distribution in human bone biopsies. *Bone*. 1998;23(4):319–326. https://doi.org/10.1016/S8756-3282(98)00112-4

14. Stockhausen KE, Qwamizadeh M, Wölfel EM, et al. Collagen fiber orientation is coupled with specific nano-compositional patterns in dark and bright osteons modulating their biomechanical properties. *ACS Nano*. 2021;15(1):455–467. https://doi.org/10.1021/acsnano.0c04786

15. Prasad KC, Kamath MP, Reddy KJM, Raju K, Agarwal S. Elongated styloid process (Eagle's syndrome): a clinical study. *J Oral Maxillofac Surg*. 2002;60(2):171–175. https://doi.org/10.1053/joms.2002.29814

16. Saccomanno S, Quinzi V, D'Andrea N, Albani A, Coceani Paskay L, Marzo G. Traumatic events and Eagle syndrome: is there any correlation? A systematic review. *Healthcare*. 2021;9(7):825. https://doi.org/10.3390/healthcare9070825

17. Chen J, Sun T, You Y, Wu B, Wang X, Wu J. Proteoglycans and glycosaminoglycans in stem cell homeostasis and bone tissue regeneration. *Front Cell Develop Biol*. 2021;9:9. https://doi.org/10.3389/fcell.2021.760532

18. Kierdorf U, Stock SR, Gomez S, Antipova O, Kierdorf H. Distribution, structure, and mineralization of calcified cartilage remnants in hard antlers. *Bone Rep*. 2022;16:101571. https://doi.org/10.1016/j.bonr.2022.101571

19. Zimmermann EA, Schaible E, Gludovatz B, et al. Intrinsic mechanical behavior of femoral cortical bone in young, osteoporotic and bisphosphonate-treated individuals in low- and high energy fracture conditions. *Sci Rep*. 2016;6(1):21072. https://doi.org/10.1038/srep21072

20. Ries C, Boese CK, Stürznickel J, et al. Age-related changes of micro-morphological subchondral bone properties in the healthy femoral head. *Osteoarthr Cartil*. 2020;28(11):1437–1447. https://doi.org/10.1016/j.joca.2020.08.001

21. Schmidt FN, Zimmermann EA, Campbell GM, et al. Assessment of collagen quality associated with non-enzymatic cross-links in human bone using Fourier-transform infrared imaging. *Bone*. 2017;97:243–251. https://doi.org/10.1016/j.bone.2017.01.015

22. Mansour S, Magnan J, Haidar H, Nicolas K, Louryan S. Comprehensive and clinical anatomy of the middle ear. 2013; Springer, Berlin, Heidelberg.

23. Breeland G, Sinkler MA, Menezes RG. *Embryology, Bone Ossification*. Treasure Island (FL): StatPearls Publishing Copyright © 2023: StatPearls Publishing LLC; 2023.

24. Kim SM, Seo MH, Myoung H, Choi JY, Kim YS, Lee SK. Osteogenetic changes in elongated styloid processes of Eagle syndrome patients. *J Craniomaxillofac Surg*. 2014;42(5):661–667. https://doi.org/10.1016/j.jcms.2013.09.012

25. Karssemakers LHE, Nolte JW, Rehmann C, Raijmakers PG, Becking AG. Diagnostic performance of SPECT–CT imaging in unilateral condylar hyperplasia. *Int J Oral Maxillofac Surg*. 2023;52(2):199–204. https://doi.org/10.1016/j.ijom.2022.08.002

26. Karssemakers LHE, Nolte JW, Tuinzing DB, Langenbach GEJ, Becking AG, Raijmakers PG. Impact of bone volume upon condylar activity in patients with unilateral condylar hyperplasia. *J Oral Maxillofac Surg*. 2018;76(10):2177–2182. https://doi.org/10.1016/j.joms.2018.03.023